JOURNAL OF MATERIALS SCIENCE **34** (1999) 6169–6176

In Situ synthesis of TiN-reinforced Si_3N_4 matrix composites using Si and sponge Ti powders

B.-T. LEE
Department of Materials Engineering, Kongju National University, 182 Sinkwan-Dong, Kongju City, 314-701, South Korea

H.-D. KIM
Ceramic Materials Group, Korea Institute of Machinery and Materials, 66 Sangnam-Dong, Chanwon, 641-010, South Korea
E-mail: lbt@knu.kongju.ac.kr

Dense Si_3N_4-TiN composites from Si and sponge Ti (0–40 wt %) powders were produced by *in situ* reaction-bonding and post-sintering under N_2 atomosphere. The fracture strength and toughness of Si_3N_4-17% TiN composite were found to be 537.9 MPa and 10.4 MPa $m^{1/2}$, respectively. In the reaction-bonded bodies, Si_3N_4 grains were constructed with α- and β-Si_3N_4 structure as well as TiN and some amounts of residual Si phase. After post-sintering, the residual Si and α-Si_3N_4 grains were transformed to β-Si_3N_4 grains with rod-like shape. No intermetallic compounds (e.g., $TiSi_2$, Ti_5Si_3 and Ti_5Si_4) were formed at the interfaces between Si_3N_4 and TiN grains. The main toughening mechanisms were crack deflection and crack bridging caused by rod-like Si_3N_4 grains which were randomly dispersed in sintered body. Microcracking due to the dispersion of *in situ* formed TiN particles also contributed to the toughening of the sintered body. © *1999 Kluwer Academic Publishers*

1. Introduction

Although Si_3N_4 ceramic has excellent mechanical properties such as fracture toughness and strength compared with other ceramics, it is not so widely used as industrial material except for the cutting tools and some engine components. The main reason is the high cost and low fracture toughness of Si_3N_4 sintered body compared with metallic systems.

Reaction-bonded silicon nitride (RBSN) which has some advantages such as low price of raw powders, easy control of dimensions and low cost of production, has been actively developed since early 1970's. However, the existence of residual Si phases and high porosity of the RBSN bodies limit the application of RBSN materials. Recently, RBSN has been re-illuminated since the removal of residual Si and pores has been made possible by post-sintering process. Furthermore, the shape of Si_3N_4 grains in the Si_3N_4 sintered body can be easily controlled by the high temperature process. In order to improve the mechanical properties of monolithic Si_3N_4 ceramic, various types of SiC [1–3], ZrO_2 [4–6] and TiN [7–12] powders were used as toughening agents. Among these, TiN particles have been found to be particularly useful due to the microcracking mechanism when optimum amounts of TiN particles are dispersed in Si_3N_4 matrix. Up to now, there are three processing routes of making Si_3N_4-TiN composites. The first method is a conventional liquid phase sintering using mixtures of Si_3N_4, TiN and some amounts of sintering additives [7, 8]. The second one is a CVD method using a gaseous mixture of SiC_{14}-TiC_{14}-NH_3-H_2 [9]. In this case, the nanometer-sized TiN crystallines dispersed in the Si_3N_4 matrix grains interact with cracks, generating crack bridging and microcracking [10]. The third process is a reaction-bonding technique using a mixture of Si, TiN and some contents of sintering additives [11, 12] In this work, the synthesis of Si_3N_4-TiN composite from Si and sponge Ti powders was carried out by the *in situ* reaction-bonding followed by gas pressure sintering technique. The purpose of the present work is to investigate the crystal structure of Si_3N_4, the relationships between microstructure and material properties of the *in situ* reaction-bonded-bodies which depend on the sintering conditions, Ti contents, and the gas-pressure. The sintered Si_3N_4-TiN composites were examined by optical microscope (OM), X-ray diffractometer (XRD), transmission electron electron microscopy (TEM) and scanning electron microscopy (SEM).

2. Experimental

Fig. 1 shows SEM micrographs of Si with irregular shapes (a) and Ti powders with sponge type (b) used in present work. The average size of Si powders used was 10 μm, but large-sized particles (about 20 μm) were also observed. The average size of Ti powder particles was about 100 μm. Some Ti powders agglomerated with fine particles were also observed as indicated with arrow heads. The Si, sponge Ti powders (0–40 wt %) and sintering additives (5 wt % Y_2O_3 and

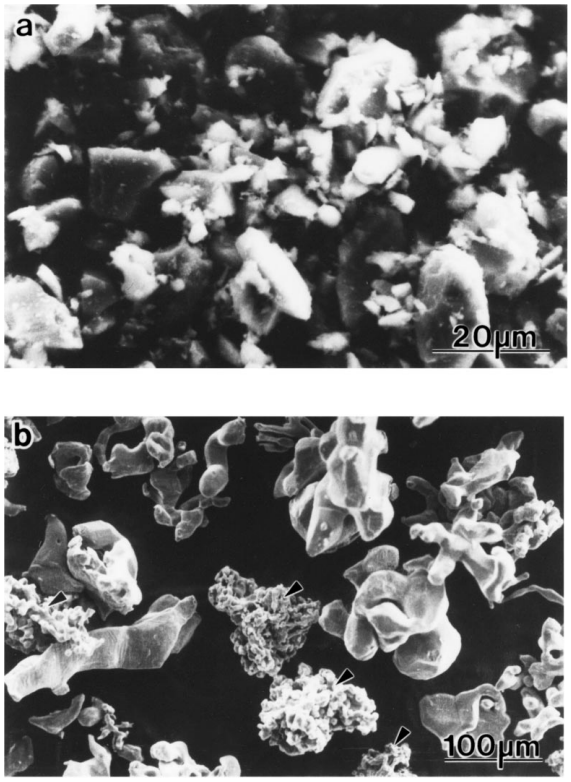

Figure 1 SEM micrographs of Si (a) and sponge Ti (b) powders.

2 wt % Al_2O_3) were throughly mixed in ethanol using a planetary ball mill and Si_3N_4 balls as milling media. The mixtures were dried on a hot plate while stirring. The powder mixture was pressed into pellets and CIPed at 250 MPa. The pellets, 40 mm in diameter were nitrided in flowing N_2-10%H_2 gas mixture at 1350 °C for 10, 20 and 30 h. To improve the mechanical properties of a nitrided momolithic Si_3N_4 and a Si_3N_4-17%TiN composite made at 1350 °C for 20 h, the post-sintering was carried out at 2000 °C for 3.5 h under 66 MPa N_2 gas pressure. The residual Si, TiN phases and porosity were identified by OM. The XRD and SEM (JSM-5300) were used to examine crystal structure and morphology of fracture surfaces of the Si_3N_4-TiN composite over a wide scale. Using TEM (JEM-2000EX), the detailed crystal structures, internal microstructure and interfacial structure between Si_3N_4 and TiN phases were examined. TEM observation was performed with a 200 kV electron microscope. The average Vickers hardness was measured by indenting with a load of 9.8N (30 points/a sample), while the average bending strength was measured by 3-point bending method at a crosshead speed of 0.5 mm/min using each 6 specimens with 3 × 4 × 30 mm bars. The fracture toughness K_{IC} was calculated by indentation method with a load of 294N [13].

3. Results and discussion

3.1. Microstructure and material properties of reaction-sintered Si_3N_4-TiN composites

Fig. 2 is optical micrographs showing the polished surfaces of samples of Si_3N_4-TiN composites reaction-bonded at 1350 °C for 20 h. In these images, the regions of black and white contrasts correspond to residual pores and Si phase, respectively. As can be seen in this images, a relatively small amount of residual Si particles were observed in Si_3N_4-17%TiN composite. The residual Si phase was remarkably higher in samples with higher Ti contents. Many residual Si particles about 7 μm size were observed with white contrasts in the Si_3N_4-35%TiN composite. The relatively poor

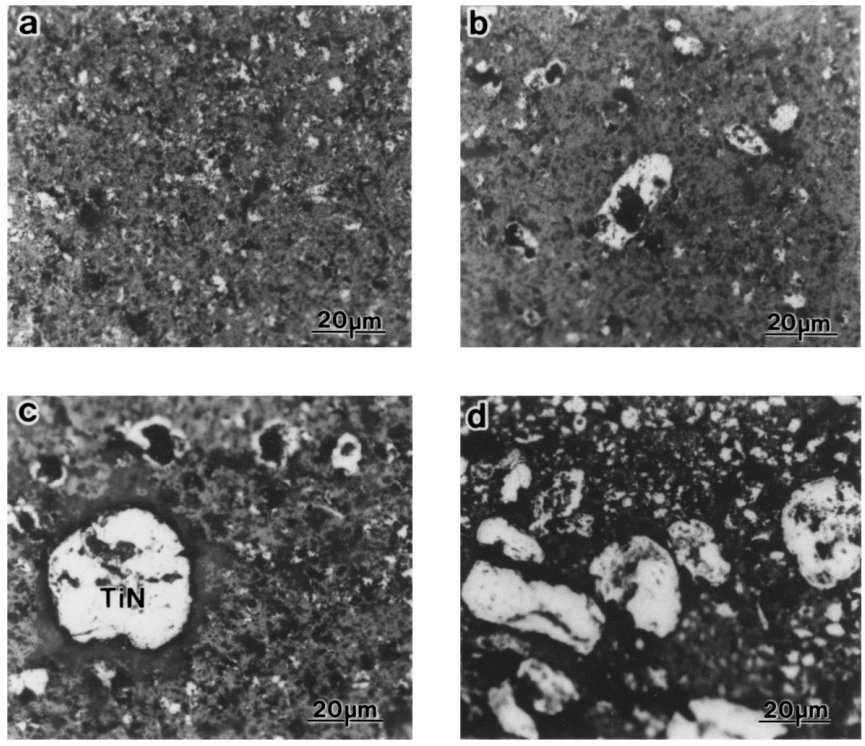

Figure 2 Optical micrographs showing the TiN phase in the reaction-bonded Si_3N_4-TiN composites at 1350 °C for 20 h. (a): Si_3N_4-0%TiN, (b): Si_3N_4-17%TiN, (c): Si_3N_4-26%TiN, (d): Si_3N_4-35%TiN.

nitridation of matrix in the Si_3N_4-35%TiN composite can probably be attributed to the followings; N_2 gas preferably reacts with Ti particles than Si powder. The other reason may be due to the excessive overheating during the nitridation as a result of the exothermic nature of the process. Melting of Si powders may lead to a blockage of pore channels, thus making it difficult for N_2 gas to penetrate the compact. Although in the black and white image, the residual Si and TiN phases do not clearly distinguish, when we observed the OM, the residual Si and TiN particles were seen with white and yellow contrasts, respectively. The OM observation of the reaction-bonded bodies confirmed that many raw Ti powders with about 100 μm were broken down to about 25 μm and well dispersed in Si_3N_4 matrix. As can be seen in Fig. 2b,c and d, most of the TiN particles contained a few of large pores, and many large crevices caused by the falling off of Si_3N_4 grains during the polishing.

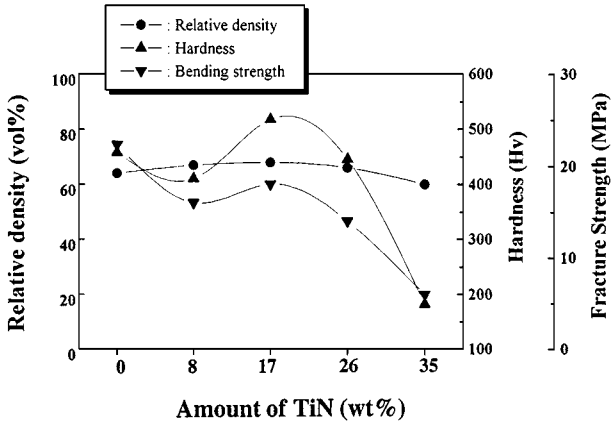

Figure 3 Ti contents dependency of relative density, Vickers hardness and bending strength in reaction-bonded Si_3N_4-TiN composites at 1350 °C for 20 h.

Fig. 3 shows relative density, Vickers hardness and bending strength of Si_3N_4-TiN composites after reaction-bonding as a function of TiN contents. As can be seen in this graph, the values of relative density and hardness showed a maximum of about 68% and 520 Hv respectively in the Si_3N_4-17%TiN composite. However, in the comparison with other available data on reaction-bonded Si_3N_4, these values are very low [11]. A general decline in properties was observed in samples containing more than 17%TiN. This behavior was due to low density and the existence of large amount of residual Si phase. The existence of microcracks of residual Si particles in the reaction-bonded body also contributed to the deterioration of the material properties [14].

Fig. 4 shows the SEM fracture surfaces made by 3-point bending test. As can be seen in the monolithic Si_3N_4 body (a), the fracture surface looked more flater than that of TiN-dispersed Si_3N_4 sintered body (c and e). In the enlarged image (b), residual pores and Si

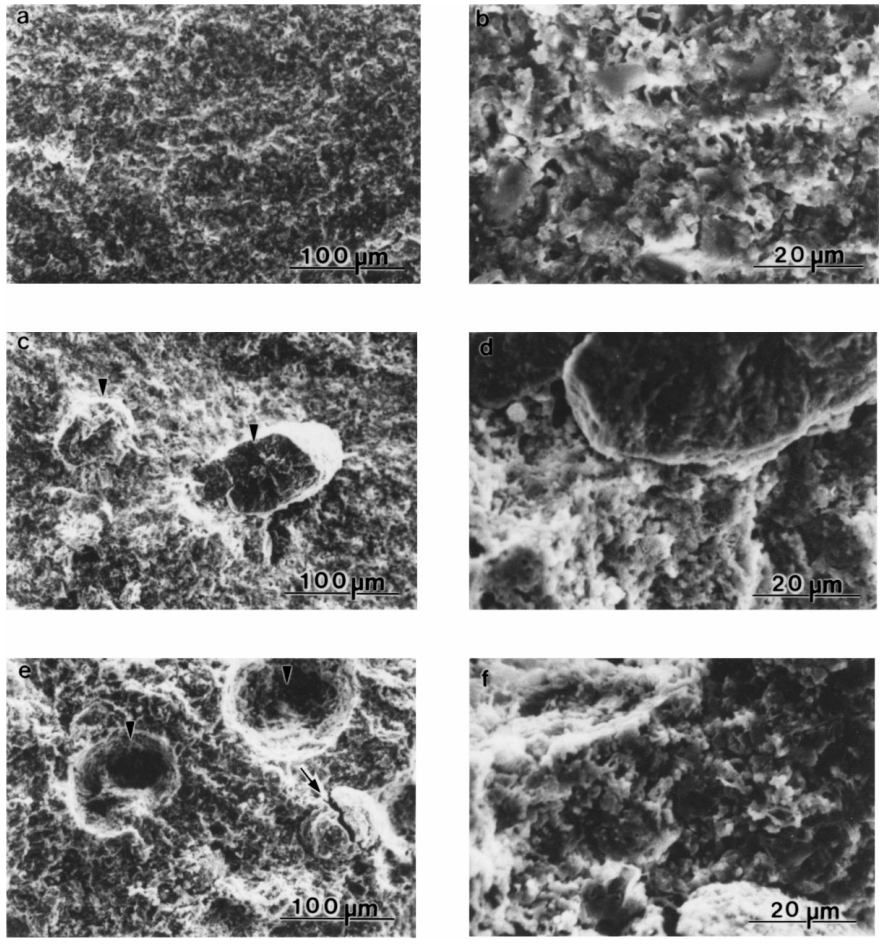

Figure 4 SEM images showing fracture morphology of reaction-bonded Si_3N_4-TiN composites at 1350 °C for 20 h. (a): Si_3N_4-0%TiN, (c): Si_3N_4-17%TiN, (e): Si_3N_4-26%TiN. (b), (d) and (f): Enlarged micrographs of (a), (c) and (e), respectively.

particles which appeared with cleavage fracture are also observed. In the 17%TiN composite (c and d), only a few residual Si particles were observed as seen in Fig. 2. Pull-out behavior of TiN particles appeared in the TiN-dispersed Si_3N_4 composites, so that TiN particles and traces of TiN particles as indicated with arrowheads (c and e) are frequently observed on the fracture surfaces. Most of the pulled-out TiN particles were very large in size about 100 μm, however some trans-granular fractures also occurred in small sized-TiN particles. A few of residual cracks in the TiN particles were observed as indicated with an arrow.

Fig. 5 shows optical micrographs of reaction-bonded Si_3N_4-17%TiN composite as a function of reaction time at 1350 °C. In the sample nitrided for 10 h, many fine residual Si phase with white contrast were observed around coarse TiN particles, but the residual Si phase showed a tendency to diminish with increasing reaction times. Also, many pores were observed as indicated with arrowheads. On the other hand, the TiN particles with large size seem to become dense particles as reaction time gradually increases. The regions with gray colour inside the coarse TiN particles corresponded to Si_3N_4 phase in which Si particles were possibly introduced into the sponge Ti particles during the ball milling process. In order to investigate whether the intermetallic compounds such as $TiSi_2$, Ti_5Si_3 and Ti_5Si_4 were formed during the reaction sintering or not, we carried out the X-ray diffraction as a dependency of reaction time.

Fig. 6c,d and e are XRD profiles of the reaction-bonded Si_3N_4-20%TiN composite at 1350 °C for 10, 20, 30 h, respectively. For a comparison, XRD profiles of raw Si (a) and sponge Ti (b) are also inserted. As can be seen in diagram, the intensity of residual Si crystals gradually decreased with increasing reaction times, however some residual Si peaks were observed after reaction-bonding for 30 h. Observations of the

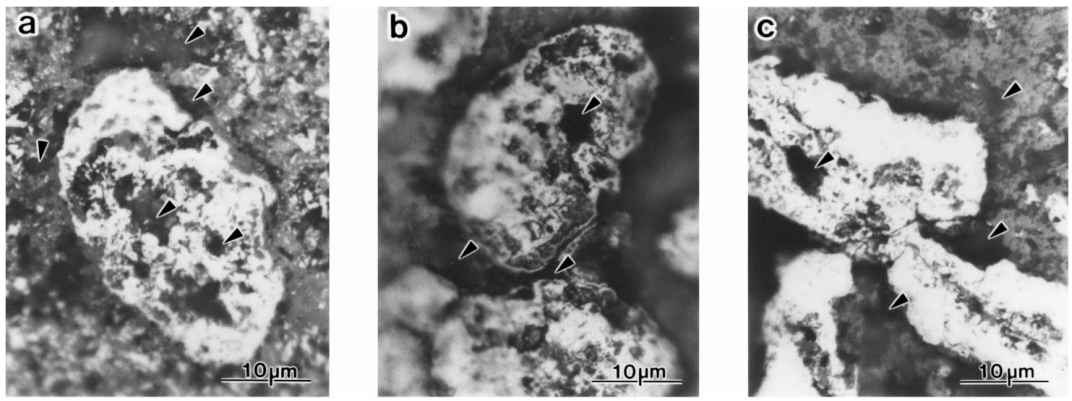

Figure 5 Optical micrographs showing TiN phase in reaction-bonded Si_3N_4-17%TiN composite at 1350 °C. (a): For 10 h, (b): For 20 h, (c): For 30 h.

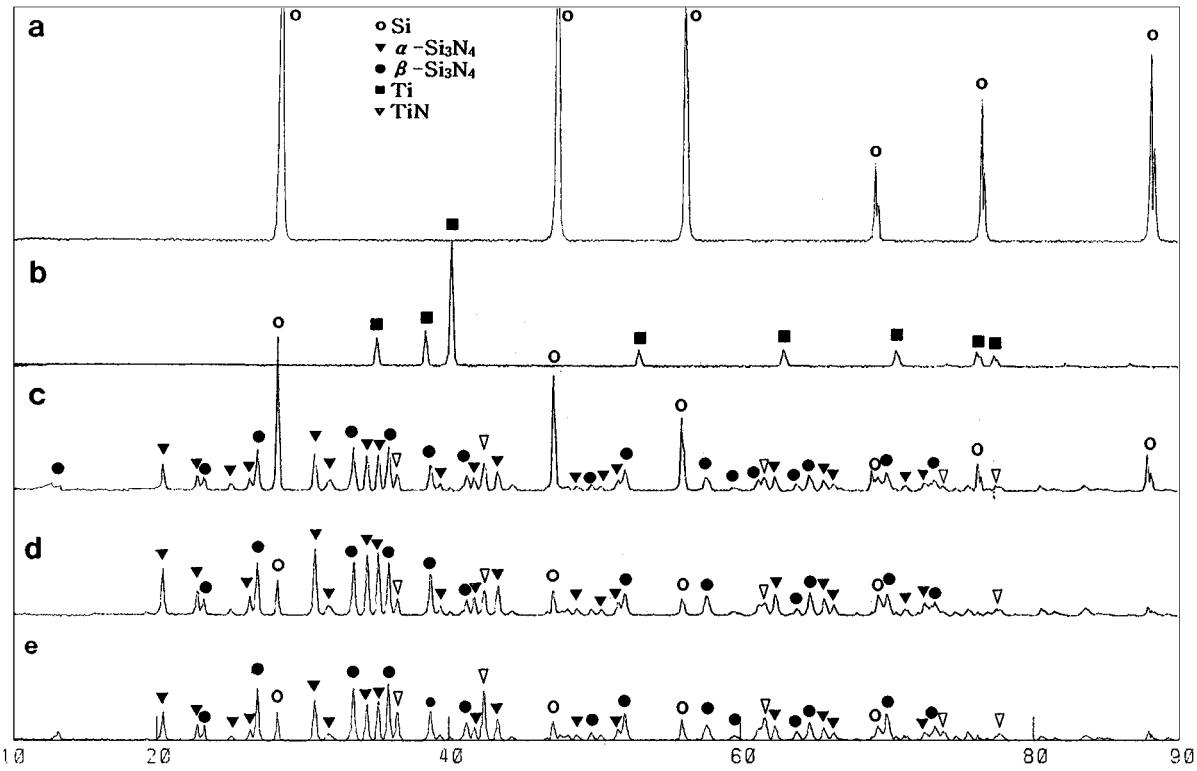

Figure 6 X-ray diffraction patterns of reaction-sintered Si_3N_4-17%TiN composites at 1350 °C. (a): Raw Si powders, (b): Raw Ti powders, (c): For 10 h, (d): For 20 h, (e): For 30 h.

crystal structure of reaction-bonded Si_3N_4 phase indicated that irrespective of the duration of the reaction α- and β-types always coexisted in the sample. From our recent TEM work on the reaction-bonded Si_3N_4 body [14], it is confirmed that α-Si_3N_4 phases are directly formed by nitridation of Si particles. In this case, cracks and dislocations in the Si particles play an important role to explain the nitridation mechanism of large sized Si particles. Generally, when the Si particles are nitrided to Si_3N_4 phase, it is well known that the Si coated with an amorphous oxide film are first decomposed, and then, Si_3N_4 nuclei are formed on the surfaces of Si particles [15]. As the nuclei gradually grow with submicron-sized α-Si_3N_4 grains, dislocations density in the Si particles increases and continuously piled up [14]. Microcracks are generated at the pile-up regions of dislocation by the lattice mismatch between α-Si_3N_4 and Si, and these microcracks gradually penetrate into all regions of Si particles with increasing sintering time [14]. This facilitates the supply of N_2 gas into interior part of Si crystals, leading to the acceleration of the nitridation process. In addition, needle-like β-Si_3N_4 crystals were also observed around comparatively large-sized pores [14]. This indirectly means that β-Si_3N_4 grains can easily be formed without the existence of a compressive effect. On the other hand, the intermetallic compounds (e.g., $TiSi_2$, Ti_5Si_3 and Ti_5Si_4) which were expected for plastic deformation toughening were not detected. The residual Ti peaks were not observed in the reaction-sintered body even after 10 h (c), and this result indicates that sponge Ti particles are easily nitrided than Si particles.

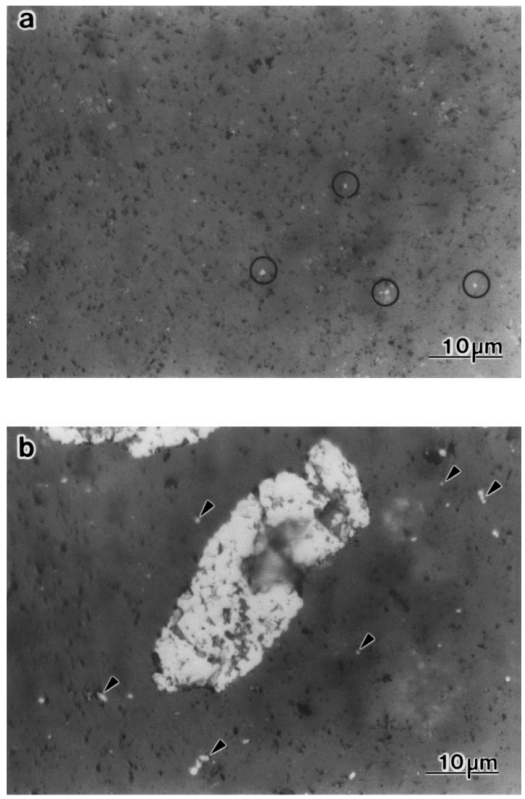

Figure 7 Optical micrographs GPSed monolithic Si_3N_4 (a) and Si_3N_4-17%TiN composite (b) at 2000 °C for 3.5 h. A few of residual Si phase are observed in the dark circled regions. Arrowheads indicate fine sized TiN particles.

3.2. Microstructure and material properties of post-sintered monolithic Si_3N_4 and Si_3N_4-17%TiN composite at 2000 °C for 3.5 h

Fig. 7 shows the polished optical micrographs of GPSed monolithic Si_3N_4 and Si_3N_4-17%TiN composite. In the monolithic Si_3N_4 body, a few of residual Si particles with less than 0.5 μm were observed with white contrast at the interior region of sintered body as indicated with dark circles, but no such observation was made on the out-side regions. In the Si_3N_4-17%TiN composite, the residual Si particles were not observed even on the interior regions. The TiN particles homogeneously dispersed in the Si_3N_4 matrix existed with two types. One type is the large sized particles which contained a few residual pores and Si_3N_4 phase, the other is the spherical shape with less than 0.7 μm in size as indicated with arrowheads. The latter is formed by the breakdown of the fine sponge-type Ti particles which was seen in Fig. 1b. A few residual Si in Fig. 7a and spherical TiN particles in Fig. 7b were distinguished by colour, that is, they were seen with white and yellow contrasts, respectively.

Fig. 8 shows XRD profiles of GPSed monolithic Si_3N_4 (a) and Si_3N_4-17%TiN composite (b). Most of

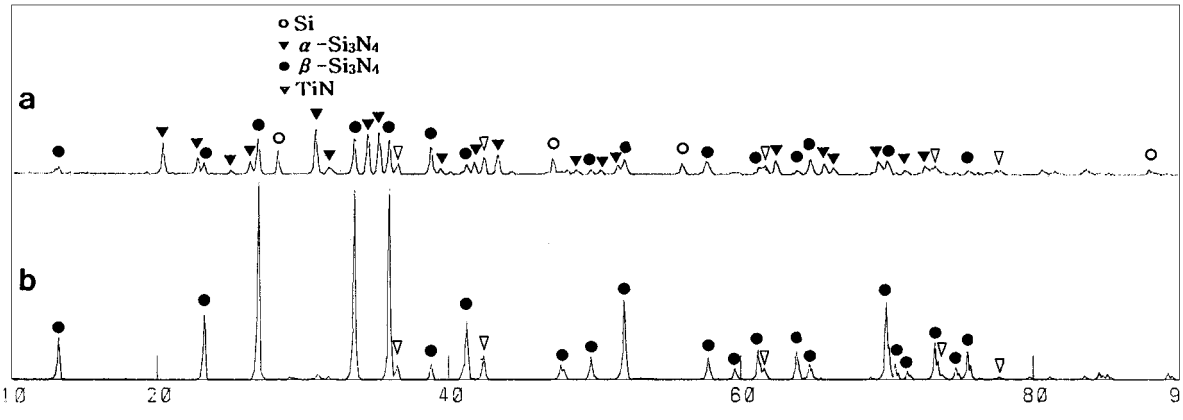

Figure 8 X-ray diffraction patterns of Si_3N_4-TiN body. (a): Reaction-sintered at 1350 °C for 20 h, (b): Reaction-sintered and GPSed at 2000 °C for 3.5 h.

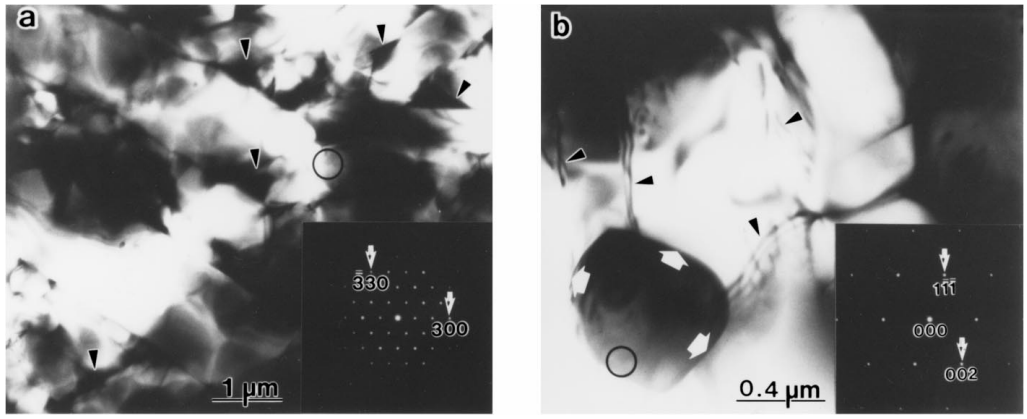

Figure 9 (a) Typical TEM image of GPSed Si_3N_4-17%TiN composite. Arrowheads indicate the existence of amorphous phase at the triple regions. (b) TEM image showing the fine sized TiN particle. Arrowheads indicate many dislocation contrasts.

residual Si phases which existed in reaction-bonded bodies (in Fig. 6) were nitrided during the GPS process, leading to elimination of Si peaks in the XRD pattern. Only β-type Si_3N_4 and NaCl type TiN peaks were detected in the XRD patterns. These results indicate that the GPS process facilitate the nitridation of residual Si phase. In addition, α-Si_3N_4 crystals were fully transformed to β-Si_3N_4 crystals during the high temperature post-sintering process.

Fig. 9 shows TEM images of GPSed Si_3N_4-17%TiN composite, and the corresponding electron diffraction patterns taken from the dark circles. As can be seen in Fig. 9a, the rod-like shaped grains about 1.5 μm in diameter were observed, and some fine sized Si_3N_4 crystals of about 0.5 μm diameter were also observed between them. The inserted electron diffraction pattern taken from a fine sized Si_3N_4 grain shows [001] zone axis of β-Si_3N_4. As frequently observed in hot-pressed Si_3N_4 body [2], the amorphous regions as marked with arrowheads were located at the triple points and grain boundaries. Fig. 8b is an enlarged TEM image showing a spherical TiN particle embedded in a Si_3N_4 grain, and an electron diffraction pattern shows [110] zone axis of TiN phase. As can be seen in this image, a few dislocations originating from TiN particles were observed in Si_3N_4 grains. From the observations made of the large dislocation lines, it is quite clear that they were formed during the cooling process after sintering, which caused a mismatching of thermal expansion coefficients and lattice parameters between Si_3N_4 and TiN particles. Generally, Si_3N_4 ceramic does not easily deform at room temperature. From our recent works on the fracture characteristic of Si_3N_4 matrix composites [2, 3, 6, 10], it was confirmed that when a crack made by indentation propagates into Si_3N_4 sintered body, some partial dislocations occur near crack process and tip zones. Observation of interfaces between Si_3N_4 and TiN particles as marked with white arrows in Fig. 9b indicated that no intermetallic compounds are formed for the reaction process. Interfaces of Si_3N_4-TiN composites synthesized by CVD process, also showed the incoherent interfacial structure without any reaction phases [10]. However, it is well known that Si_3N_4 ceramic is very reactive with Al alloys [16, 17]. For an example, in the Si_3N_4 whisker-reinforced 7074Al matrix composite, many β-Mg_2SiO_4 reaction compounds about 40 nm were formed at the interfaces between 7064Al and Si_3N_4 whisker [17]. The existence of nitrogen atmosphere during the reaction bonding process probably explains why no intermetallic compounds were formed. Our TEM observations confirmed that large TiN particles were the result of an agglomeration of polycrystals of TiN particles containing some residual pores and Si_3N_4 phases. Microcracks were not observed around TiN particles.

TABLE I Material properties of GPSed monolithic Si_3N_4 and Si_3N_4-TiN composites (at 2000 °C for 3.5 h)

Specimen	Relative density (%)	Hardness (kg/m^2)	K_{IC} ($MPa \cdot m^{1/2}$)	Fracture strength (MPa)
Si_3N_4-0%TiN	98.5	1486.3	7.9	495.1
Si_3N_4-17%TiN	94.8	1462.5	10.4	537.9

Table I shows the material properties of GPSed monolithic Si_3N_4 and Si_3N_4-17%TiN composite. The relative densities of monolithic Si_3N_4 and Si_3N_4-17%TiN composite are 98.5 and 94.8%, respectively. Inspite of low relative density and existence of large sized TiN particles in the Si_3N_4-17%TiN composite, the values of hardness and fracture strength are 1462.5 kg/mm^2 and 537.9 MPa. In particular, the average fracture toughness measured by indentation method also shows very high value of 10.4 $MPam^{1/2}$.

Fig. 10 shows SEM fracture surfaces of GPSed monolithic Si_3N_4 (a) and Si_3N_4-17%TiN composite (b and c) made by 3-point bending test. As can be seen in both sintered bodies, the rough surfaces were observed in the fracture surfaces. This observation indicates that main fracture of both GPSed bodies was the intergranular type. On the fracture surface, there was evidence of pull-out of many rod-like β-Si_3N_4 grains with high aspect ratio and their traces. This is similar to an observation previously made in SiC-whisker-reinforced Si_3N_4 composite [2]. This observation indicates that the microstructural control of matrix is enhanced by the post-sintering process. The appearance of typical intergranular fracture and pull-out phenomenon of rod-like Si_3N_4 grains on the fracture surfaces indicate crack

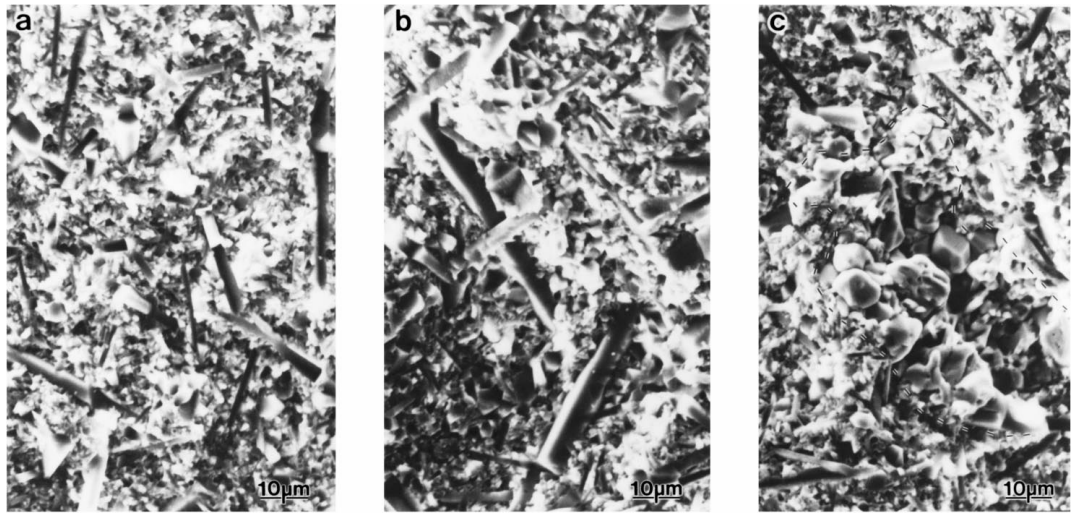

Figure 10 SEM fracture surfaces showing intergranular fracture of GPSed monolithic Si_3N_4 (a) and Si_3N_4-17%TiN composite (b and c).

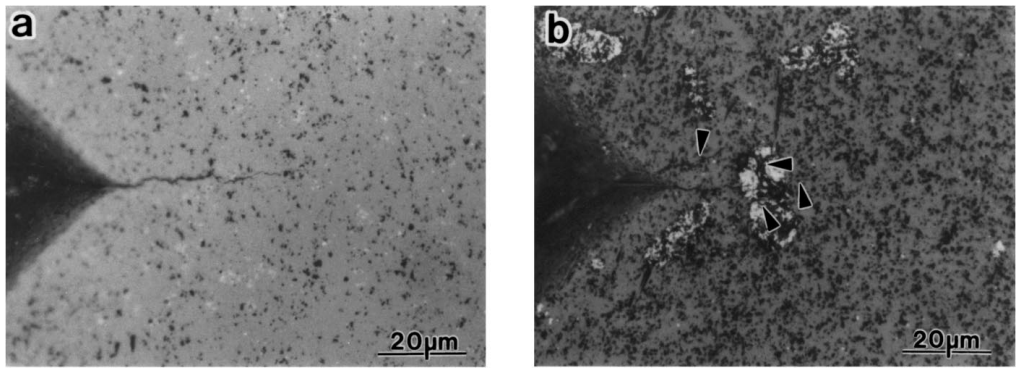

Figure 11 Optical micrographs showing crack propagation of post-sintered monolithic Si_3N_4 (a) and Si_3N_4-17%TiN composite.

deflection and crack bridging mechanisms required to improve the fracture toughness. Furthermore, in the Si_3N_4-17%TiN composite (in Fig. 10b), the diameter of rod-like Si_3N_4 grains was larger than that of monolithic Si_3N_4 grains (in Fig. 10b). Mitomo and Tajima reported that the relationship between fracture toughness and diameter of rod-like Si_3N_4 grains is such that that the toughening effects are increased with increasing average diameter of rod-like Si_3N_4 grains [18]. The dispersion of TiN particles enhances fracture toughness by microcracking due to the existence of strain fields around the TiN particles [19] as shown in Fig. 9b. In the Fig. 10c, a large-sized TiN particle with about 60 μm as indicated with a dot-lined region is intergranularly fractured, so that the sharped grains are observed. The existence of residual pores and Si_3N_4 phase in the large-sized TiN particles leads to the intergranular fracture of TiN particles.

Fig. 11 is optical micrographs showing crack propagation of GPSed monolithic Si_3N_4 and Si_3N_4-TiN composite made by Vickers indentation with a load of 294N. In Fig. 11a, a crack propagated from the diamond cone, is well observed showing some crack deflection. On the other hand, in the Si_3N_4-17%TiN composite, the main crack is very short length compared with that of monolithic Si_3N_4. In addition, microcracks are observed in the TiN particle as indicated with arrowheads. It is supposed that when a crack propagated into TiN particles, the crack propagation energy is diminished by the formation of many microcracks at the interior of TiN particles. From the above results, it is concluded that high fracture toughness in the Si_3N_4-17%TiN composite originates from the multi toughening mechanisms of crack bridging, crack deflection and microcracking.

4. Conclusions

From the present study of *in situ* synthesis of Si_3N_4-TiN composite using Si and sponge Ti powders, the following results were obtained.

(1) In the reaction bonded composites, the values of hardness and relative densities are maximum in the Si_3N_4-17%TiN composite.

(2) The dispersed Ti particles were fully nitrided to TiN phase at 1350 °C, but intermetallic compounds (e.g., $TiSi_2$, Ti_5Si_3 and Ti_5Si_4) were not formed at the interface between Si_3N_4 and TiN grains.

(3) After the post-sintering, the equiaxed α-Si_3N_4 grains that existed in the reaction-bonded bodies were transformed to rod-like β-Si_3N_4. The fracture strength of Si_3N_4-17%TiN composite was comparatively low, 537.9 MPa, but the fracture toughness was 10.4 MPa $m^{1/2}$.

(4) The fracture mode of GPSed Si_3N_4-17%TiN composite was typically intergranular, whilst the main

toughening effect was due to crack deflection and crack bridging caused by well developed rod-like Si_3N_4 grains. Microcracking caused by the difference in thermal expansion coefficient and lattice parameter between Si_3N_4 and TiN phases also contributed to the toughening of the composite.

Acknowledgement

The authors wish to acknowledge the financial support of the Korea Research Foundational made in the program year of 1997.

References

1. H. KODAMA, T. SUZUKI, H. SAKAMOTO and T. MIYOSHI, *J. Amer. Ceram. Soc*. **73** (1990) 678.
2. B. T. LEE and K. HIRAGA, *Mater. Trans. JIM* **34** (1993) 930.
3. B. T. LEE, G. PEZZOTTI and K. HIRAGA, *Mater. Sci and Eng*. **A177** (1994) 151–60.
4. F. F. LANGE, L. K. L. FALK and B. T. DAVIS, *J. Mater. Res*. **2** (1987) 66.
5. H. J. KLEEBE, W. BRAUE and W. LUXEM, *J. Mater. Sci*. **29** (1994) 1265.
6. B. T. LEE, T. KOYAMA, A. NISHIYAMA and K. HIRAGA, *Scrip. Met. et Mater*. **32** (1995) 1073.
7. T. NAGAOKA, M. YASUOKA, K. HIRA and S. KANZAKI, *J. Ceram. Soc. Jpn.* **100** (1992) 617.
8. A. BELLOSI, S. GUICCIARDI and A. TAMPIERI, *J. Euro. Ceram. Soc*. **9** (1992).
9. T. HIRAI and S. HAYASHI, *J. Mater. Sci*. **17** (1982) 1320.
10. B. T. LEE, S. HAYASHI, T. HIRAI and K. HIRAGA, *Mater. Trans. JIM* **34** (1993) 573.
11. Y. YASUTOMI, A. CHIBA and M. SOBUE, *J. Amer. Ceram. Soc*. **74** (1991) 950.
12. G. HILLINGER and V. HLAVACEK, *ibid*. **78** (1995) 495.
13. D. K. SHETTY, A. R. ROSENFIELD and W. DUCKWORTH, *ibid*. **68** (1985) C-65.
14. B. T. LEE and H. D. KIM, *Mater. Trans. JIM* **37** (1996) 1547.
15. Y. YASUTOMI, M. SOBUE, S. SHINOZAKI and J. HANGAS, *J. Ceram. Soc. Jpn.* **98** (1990) 429.
16. K. SUGANUMA, *J. Euro. Ceram. Soc*. **11** (1993) 43.
17. B. T. LEE, K. HIGASHI and K. HIRAGA, *J. Mater. Sci. Lett*. **16** (1997) 206.
18. M. MITOMO and Y. TAJIMA, *J. Ceram. Soc. Jpn*. **100** (1991) 1014.
19. B. T. LEE and H. D. KIM, Preparation Manuscript (1997).

Received 12 August 1997
and accepted 18 June 1999